Electronic Supplementary Material (ESI) for Materials Chemistry Frontiers.
This journal is © the Partner Organisations 2019

Supplementary Information for

Understanding the Operational Lifetime Expansion Methods of Thermally Activated Delayed Fluorescence Sensitized OLEDs: A Combined Study of Charge Trapping and Exciton Dynamics

Chongguang Zhao[1], *Chen Li*[1], *Yilang Li*[1], *Yong Qiu*[1] *and Lian Duan**[1,2]

[1]Key Lab of Organic Optoelectronics and Molecular Engineering of Ministry of Education, Department of Chemistry, Tsinghua University, Beijing 100084, China.

[2]Center for Flexible Electronics Technology, Tsinghua University, Beijing 100084, P. R. China.

Corresponding Author:

Lian Duan Email: duanl@mail.tsinghua.edu.cn

1. *J-V* Characteristics of Single-carrier Testing Devices.

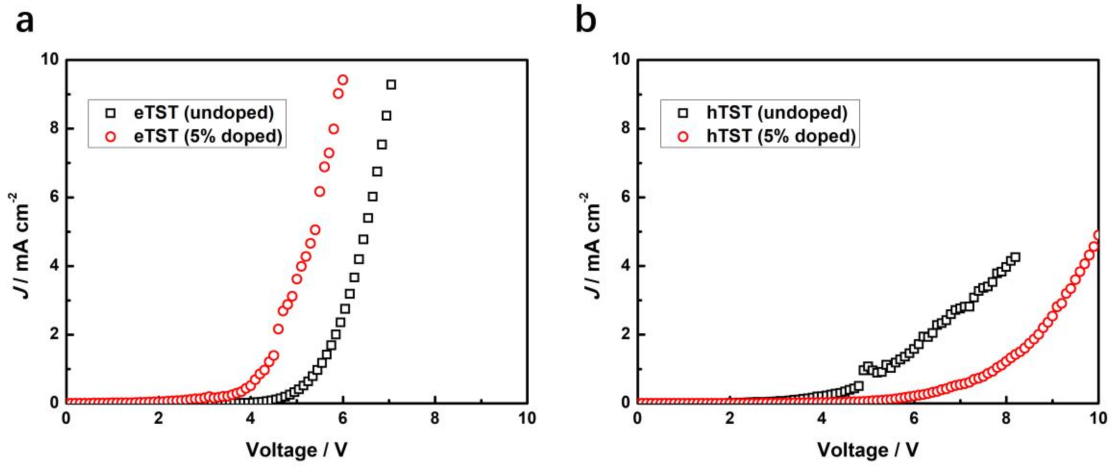

Figure S1. Non-logarithmic *J-V* Characteristics of (a) electron-only and (b) hole-only testing devices before and after doping.

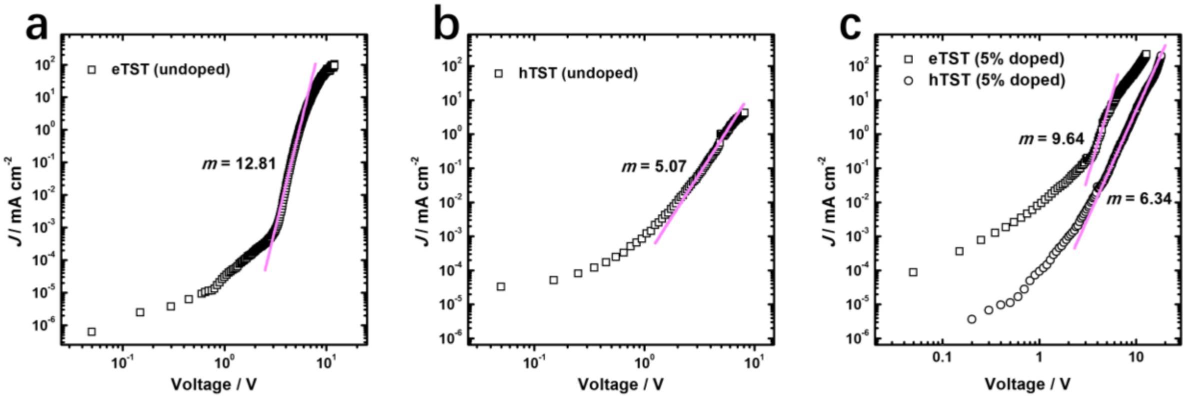

Figure S2. Fitting of the traped-charge-limited-current (TCLC) region with *J-V* relation of $J \propto V^m$, where the calculated values of *m* were shown in the figures. Each figure denotes device: (a) eTST (undoped); (b) hTST (undoped); (c) eTST (5 wt% doped) and hTST (5 wt% doped).

Table S1. The Calculated Trap Density in Each Single-carrier Devices.

	Electron-only	Hole-only
undoped	1.9×10^{17} cm^{-3}	2.1×10^{17} cm^{-3}
doped	2.1×10^{17} cm^{-3}	2.0×10^{19} cm^{-3}

The trap densities were calculated from the J-V relations of each plot in TCLC region. In this region, current density with traps is given by the Mark and Helfrich equation[1]

$$J_{\mathrm{TCLC}} = \frac{\mu N_{\mathrm{c}}}{e^{m-2}}\left(\frac{2m-1}{m}\right)^{m}\left(\frac{\epsilon_0\epsilon_{\mathrm{r}}(m-1)}{N_{\mathrm{t}}m}\right)^{m-1}\frac{V^{m}}{w^{2m-1}} \tag{S1}$$

where m is the exponential index of $J \propto V^m$ relation, N_{c} and N_{t} are the effective density of states and the total trap density, respectively. The quasi-feimi level (E_f) of the traps in the Arrhenius form of **Eq. S1** can be expressed as[1,2]

$$E_f(V) = (m-1)kT\ln\left[f(m)\frac{ew^2N_{\mathrm{t}}}{\epsilon_0\epsilon_{\mathrm{r}}V}\right] \tag{S2}$$

where $f(m) = \frac{m}{m-1}\left(\frac{m}{2m-1}\right)^{m/(m-1)}$. When all traps are filled at a critical voltage V_{c}, the quasi-fermi level would satisfy the condition of $E_f(V_{\mathrm{c}}) = 0$, the total trap density can be therefore calculated by

$$N_{\mathrm{t}} = \frac{1}{f(m)}\frac{\epsilon_0\epsilon_{\mathrm{r}}V_{\mathrm{c}}}{ew^2} \tag{S3}$$

The total trap densities in eTST (undoped), hTST (undoped) and eTST (doped) devices can be well obtained by **Eq. S3**. While for hTST (doped) device, since there is no critical voltage V_{c}, with **Eq. S3** we could only know $N_{\mathrm{t}} > 1.5\times10^{18}$ cm^{-3}, whereas the total trap density can be estimated with the fitting of **Eq. S1**, by assuming the density of state entirely effective in the conduction band.

2. Cyclic Voltammetry Measurement.

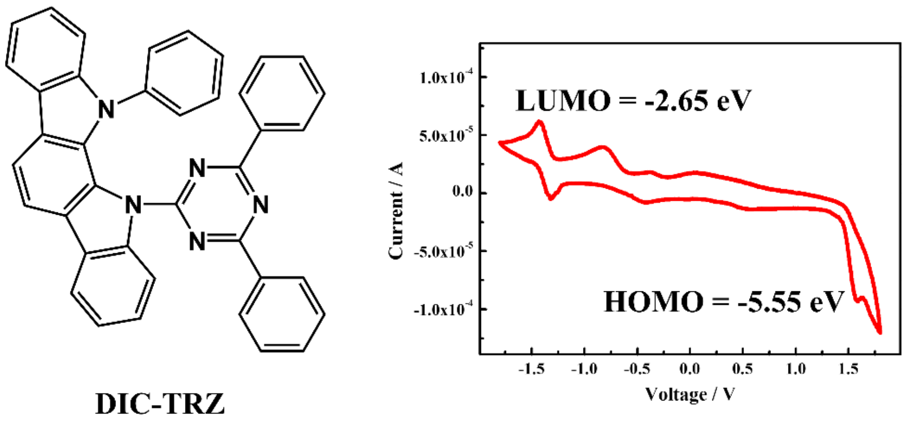

Figure S3. Molecular structure and cyclic voltammetry measurement result of DIC-TRZ.

3. Photo and Electrical Aging of Single-carrier Devices.[3]

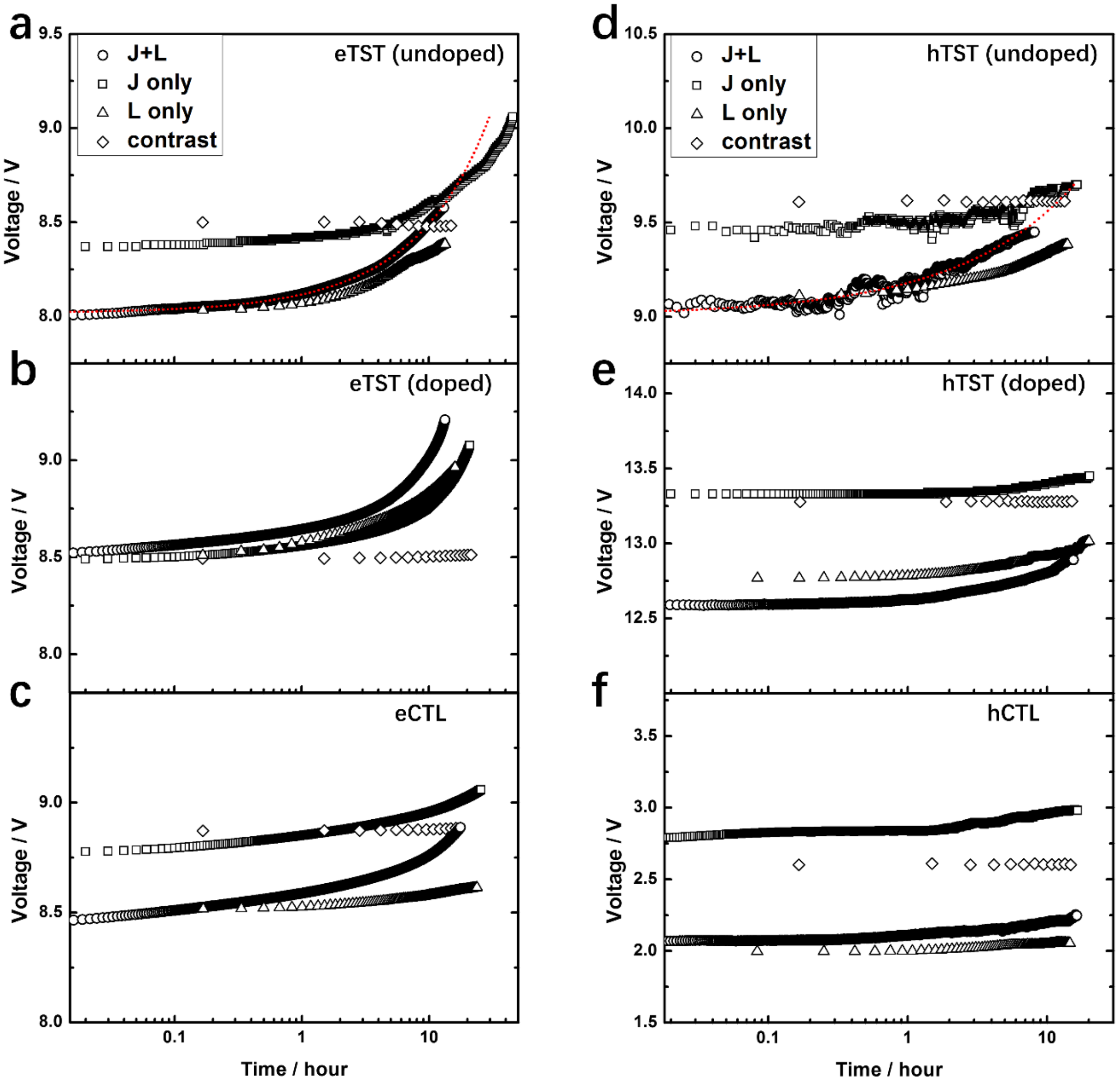

Figure S4. Driving voltage of single-carrier devices over time under various testing conditions. EODs: (a) undoped eTST, (b) 5 wt % doped eTST, (c) eCTL. HODs: (d) undoped hTST, (e) 5 wt % doped hTST, (f) hCTL. Red dotted lines indicate power-law fits of J+L conditions according to reference 3.

4. Operational Stability Comparison of the TADF Host and Conventional Host devices.

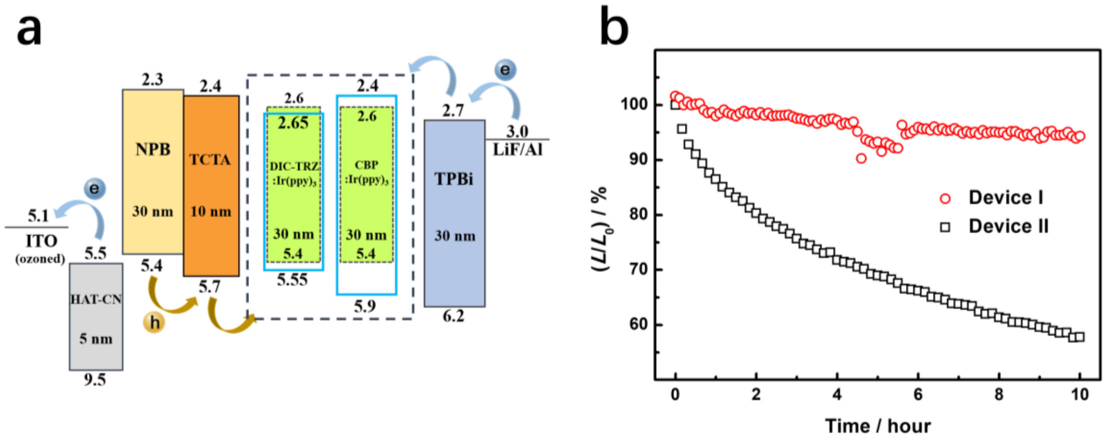

Figure S5. The (a) energy diagram and (b) luminance loss plots (measured at the constant *J* of 20 mA cm^{-2}) of Device I with TADF host and Device II with conventional host. The device structures are:

Device I: ITO substrate (80 nm) / HAT-CN (5 nm) / NPB (30 nm) / TCTA (10 nm) / DIC-TRZ : 5 wt% Ir(ppy)$_3$ (30 nm) / TPBi (30 nm) / LiF (1 nm) / Al (150 nm);

Device II: ITO substrate (80 nm) / HAT-CN (5 nm) / NPB (30 nm) / TCTA (10 nm) / CBP : 5 wt% Ir(ppy)$_3$ (30 nm) / TPBi (30 nm) / LiF (1 nm) / Al (150 nm), where CBP denotes 4,4′-Bis(carbazol-9-yl)biphenyl.

5. Extracting the Calculation Parameters from the Experimental Data.

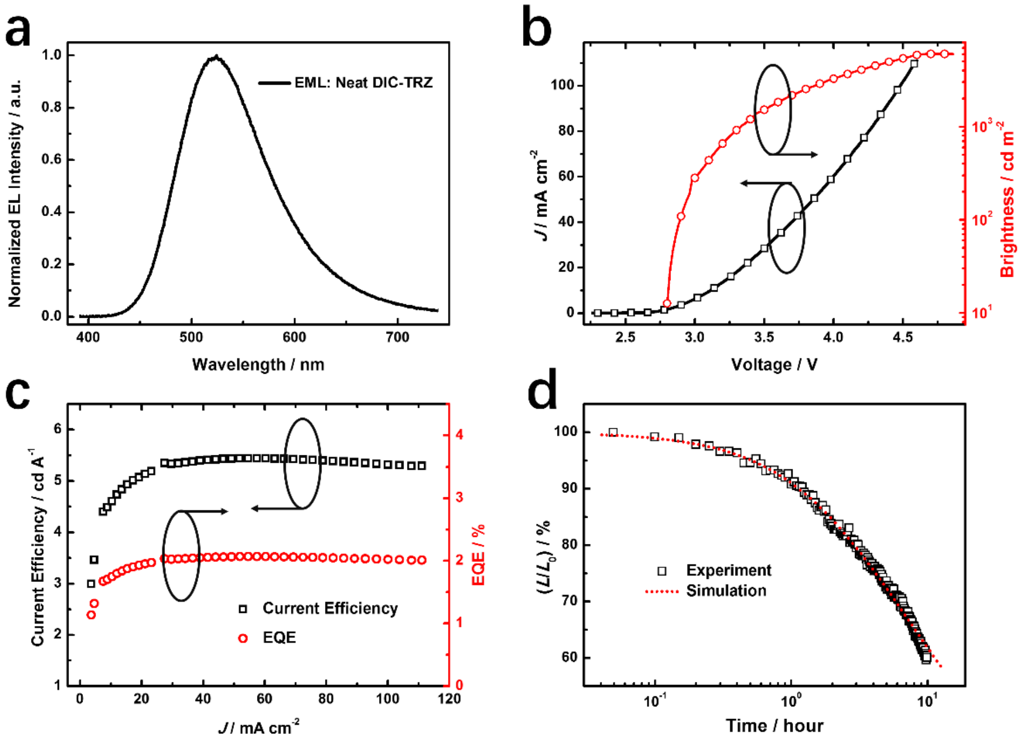

Figure S6. Performance of OLED device with structure of ITO substrate (80 nm) / HAT-CN (5 nm) / NPB (30 nm) / TCTA (10 nm) / DIC-TRZ (30 nm) / TPBi (30 nm) / LiF (1 nm) / Al (150 nm). (a) EL spectra, (b)

J-*V*-*L* curves, (c) current efficiency - *J* and EQE-*J* curves, and (d) experimental and simulated luminance loss curve, at a constant current density of 20 mA cm^{-2}. ΔE_{ST} of 0.06 eV and k_{S} from **Table S2** were used in the simulation.[4]

6. Simulated Lifetime Analysis

When k_{S} was set as 1.0×10^{8} s^{-1}, IQE as a function of operational time for TADF OLEDs under various ΔE_{ST}s was calculated and denoted in **Figure S7a**, with k_{RISC} described as $k_{\mathrm{ISC}}\exp(-\Delta E_{\mathrm{ST}}/k_{\mathrm{B}}T)$, and an initial defect density of 1.0×10^{-12} cm^{-3}.[5] The initial IQE values represent the internal quantum efficiency after efficiency roll-off under the applied current density, which well agreed with our previous simulations on device efficiency roll-off (**Figure S8**, at J = 20 mA cm^{-2}).[6] Initial IQEs (IQE$_{\mathrm{ini}}$s) approximate 100% were realized under small ΔE_{ST}s ($\leq 2k_{\mathrm{B}}T \approx 0.05$ eV), while went down along with the raise of ΔE_{ST}. At a ΔE_{ST} of $4k_{\mathrm{B}}T(\approx 0.1$ eV), IQE$_{\mathrm{ini}}$ could also approach to 100% at a smaller current density, but went under 80% at J = 20 mA cm^{-2} (**Figure S8**). When ΔE_{ST} exceeded $8k_{\mathrm{B}}T(\approx 0.2$ eV), the IQE$_{\mathrm{ini}}$s dropped close to 25%, and almost no TADF properties were exhibited. All of these are consistent with the properties of various realistic materials.[7]

Here *LT*80s were employed to characterize the operational lifetime of OLED devices. A *LT*80 of 573 h was realized at zero ΔE_{ST}, then decreased rapidly while ΔE_{ST} raised, with only 0.17 h remained at a ΔE_{ST} of $6k_{\mathrm{B}}T$. Whereas ΔE_{ST} reached and exceeded $8k_{\mathrm{B}}T$, the TADF properties almost vanished, then *LT*80 returned to increase and finally rise to a high-level when $k_{\mathrm{RISC}}\approx0$, which also corresponded to the circumstance of conventional fluorescence. In order to further investigate the origination of radiative singlets, the ratio of delayed singlet excitons was calculated and depicted in **Figure S7b**, which could be expressed as

$$\Phi_{\mathrm{d}} = \frac{k_{\mathrm{RISC}} n_{\mathrm{T}}}{\xi \gamma n_{\mathrm{P}}{}^{2} + k_{\mathrm{RISC}} n_{\mathrm{T}}} \qquad \text{(S4)}$$

And the prompt singlet ratio could thus be calculated by $\Phi_{\mathrm{p}}=1-\Phi_{\mathrm{d}}$. We noticed that inhibiting the decrease of delayed singlet ratio could alleviate the efficiency loss, leading to an enhanced operational lifetime. This could confirm that increasing the delayed part luminance could intrinsically contribute to the device stability.

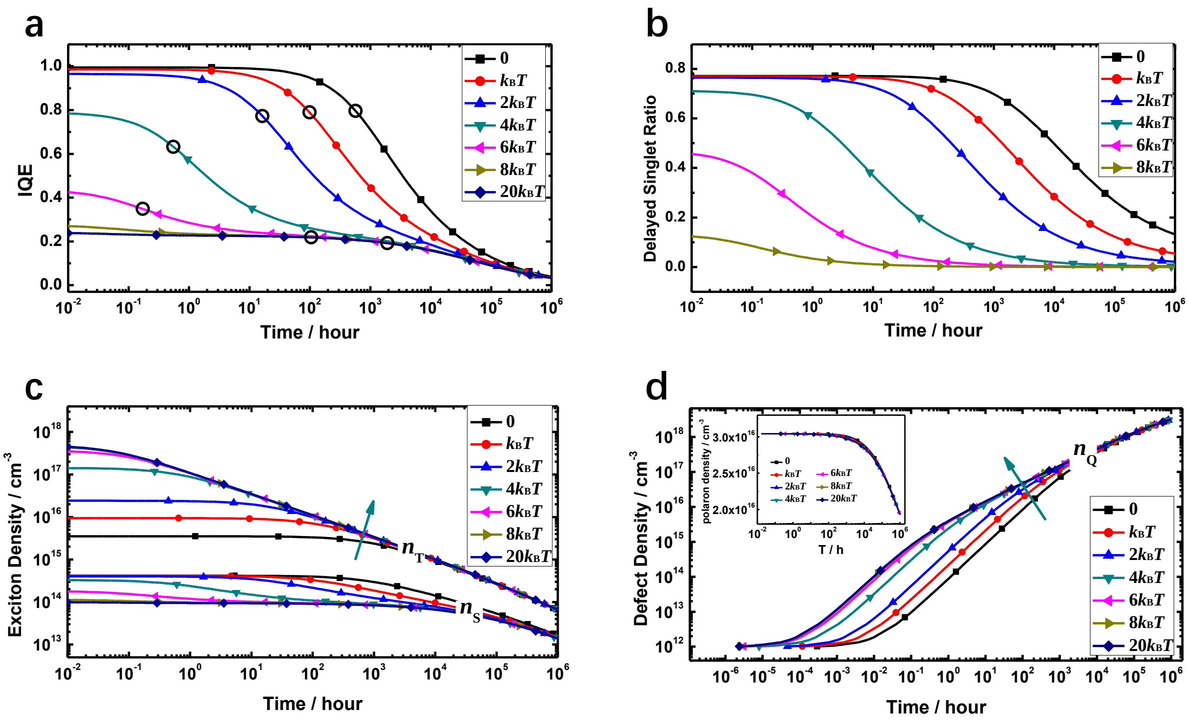

Figure S7. Simulated (a) IQE, (b) delayed singlet ratio, (c) singlet and triplet densities, and (d) defect density and polaron density (inset figure) versus operational time for TADF OLEDs under various ΔE_{ST}s at constant J of 20 mA cm^{-2}, when setting $k_{\mathrm{S}} = 1.0 \times 10^{8}\ \mathrm{s}^{-1}$. Open circles in (a) indicate the points of IQE decreased to 80% of initial level.

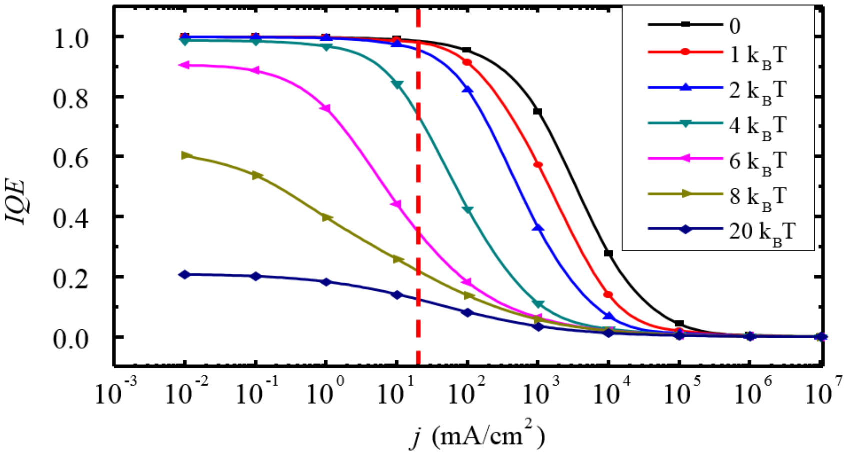

Figure S8. Simulated IQE versus current density under various ΔE_{ST}s. The red dashed line denotes j = 20 mA cm^{-2}, where is the applied current density of device lifetime simulation. IQE values under current density of 20 mA cm^{-2} in this figure are the initial IQE values in lifetime simulation before degradation.[6]

Densities of excitons, polarons, and defects over time were also tracked, shown in **Figure S7c,d**. Since the polaron density merely implemented a neglectable decrease over ΔE_{ST} (see the inset figure in **Figure S7d**), the increase of total exciton density could to a great extent give rise to the expedition of defect accumulation. Note that triplet density is one to three orders of magnitude larger than singlet density in all periods, in larger ΔE_{ST}s the growing density of triplets apparently prevailed over the reduced singlets, generating more severe exciton-polaron annihilations, thus the defect accumulation was accelerated. From the above we could indicate, the reason for longer device operational lifetime caused by smaller ΔE_{ST}s is to consume the triplets in time by achieving faster RISC, so that the defect accumulation was retarded by restricting the exciton-polaron annihilation.

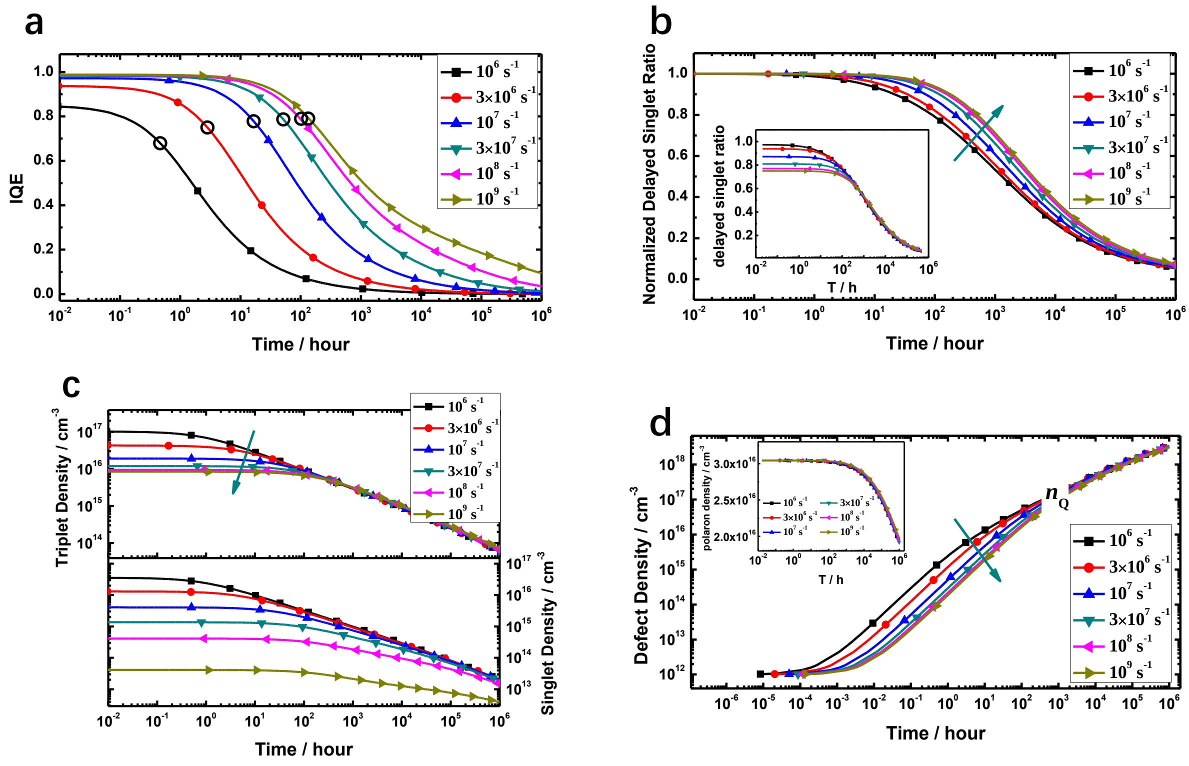

Figure S9. Simulated (a) IQE, (b) normalized and unnormalized (inset figure) delayed singlet ratio, (c) singlet and triplet densities, and (d) defect density and polaron density (inset figure) versus operational time for TADF OLEDs under various k_{S}s at constant J of 20 mA cm^{-2}, when setting $\Delta E_{\mathrm{ST}} = k_{\mathrm{B}}T$. Open circles in (a) stand for the points of IQE decreased to 80% of initial level.

Likewise, when ΔE_{ST} was setting to be $k_{\mathrm{B}}T$, IQE over time under various k_{S}s was calculated and presented in **Figure S9a**. From where we could see, the IQE$_{\mathrm{ini}}$s and $LT80$s increased with the growing k_{S}s, indicating the promoted efficiency and enhanced operational stability were achieved simultaneously at a high singlet radiative rate. Also we could deduce from **Figure S9b-d**, such effects of k_S on the device performance similarly attributes to the retarded decrease of delayed part ratio (despite the diminishment on the absolute values), inducing the more efficient consumption on triplets, defeating the neglectable increase of polarons, and finally alleviate the defect accumulation by inhibiting exciton-polaron annihilation. Since in all applied parameters the simulated triplet density is much higher than singlet density (**Figure S7c, S9c**), it is apprehensible that SSA contributes triflingly in exciton annihilations, thus the neglect of SSA is practicable.

7. Device Performance of Green TSL OLEDs.

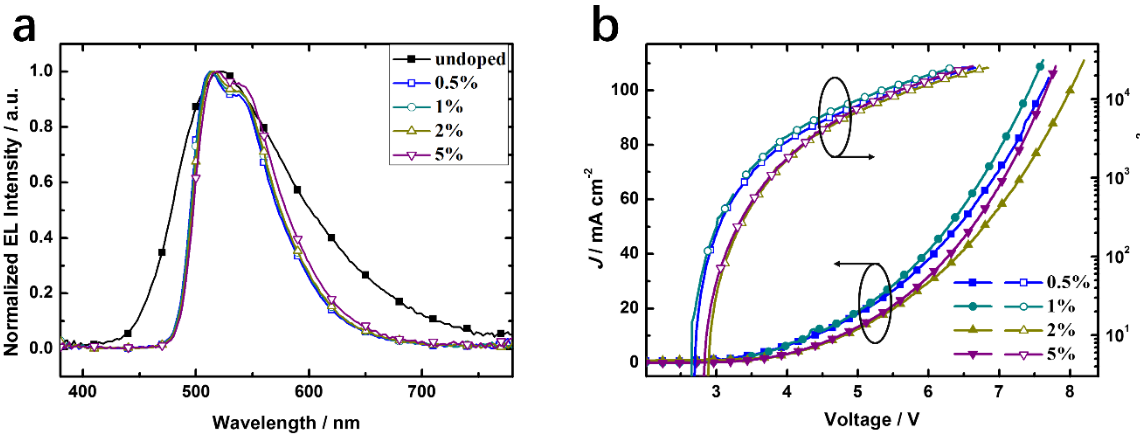

Figure S10. Performance of OLED devices with structures of ITO substrate (80 nm) / HAT-CN (5 nm) / NPB (30 nm) / TCTA (10 nm) / DIC-TRZ : *x* wt % Ir(ppy)$_3$ (30 nm) / TPBi (30 nm) / LiF (1 nm) / Al (150 nm), with various *x* of 0, 0.5, 1, 2, and 5. (a) EL spectra. (b) *J*-*V*-*L* curves.

8. Photoluminescent Transient Measurement.

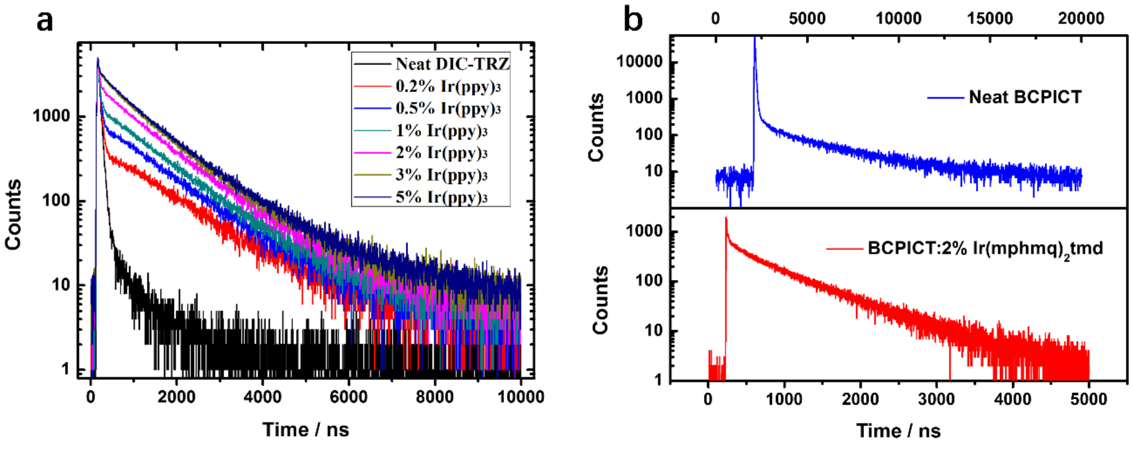

Figure S11. The photoluminescent transient curves of (a) DIC-TRZ : *x*% Ir(ppy)$_3$ and (b) BCPICT : *x*%

$Ir(mphmq)_2(tmd)$ films, collected at the respective wavelength of 520 nm and 620 nm.

Table S2. Prompt fluorescent lifetime (τ_P), energy transfer rate coefficient (k_{ET}) and fluorescent radiation rate coefficient (k_S) for the films.

Film	τ_P / ns	k_{ET} / s^{-1}	k_S / s^{-1}
Neat DIC-TRZ	56	-	3.3×10^6
DIC-TRZ:0.2%$Ir(ppy)_3$	47	3.4×10^6	
DIC-TRZ:0.5%$Ir(ppy)_3$	36	9.9×10^6	
DIC-TRZ:1%$Ir(ppy)_3$	25	2.2×10^7	
DIC-TRZ:2%$Ir(ppy)_3$	15	4.9×10^7	
DIC-TRZ:3%$Ir(ppy)_3$	12	6.5×10^7	
DIC-TRZ:5%$Ir(ppy)_3$	5.5	1.6×10^8	
Neat BCPICT	40	-	-
BCPICT:2%$Ir(mphmq)_2(tmd)$	17	3.4×10^7	

τ_Ps were extracted from the photoluminescent transient curves according to exponential fitting. k_{ET} was calculated by

$$k_{ET} = \tau_P^{-1}(\text{doped}) - \tau_P^{-1}(\text{neat})$$

k_S was calculated by

$$k_S = \tau_P^{-1}(\text{neat}) \cdot PLQY$$

where PLQY is the experimental photoluminescent quantum yield of fluorescence of DIC-TRZ film, which is measured to be 18.5%.[4,6]

9. Device Performance and Parameter Extraction of Red TSL OLED.

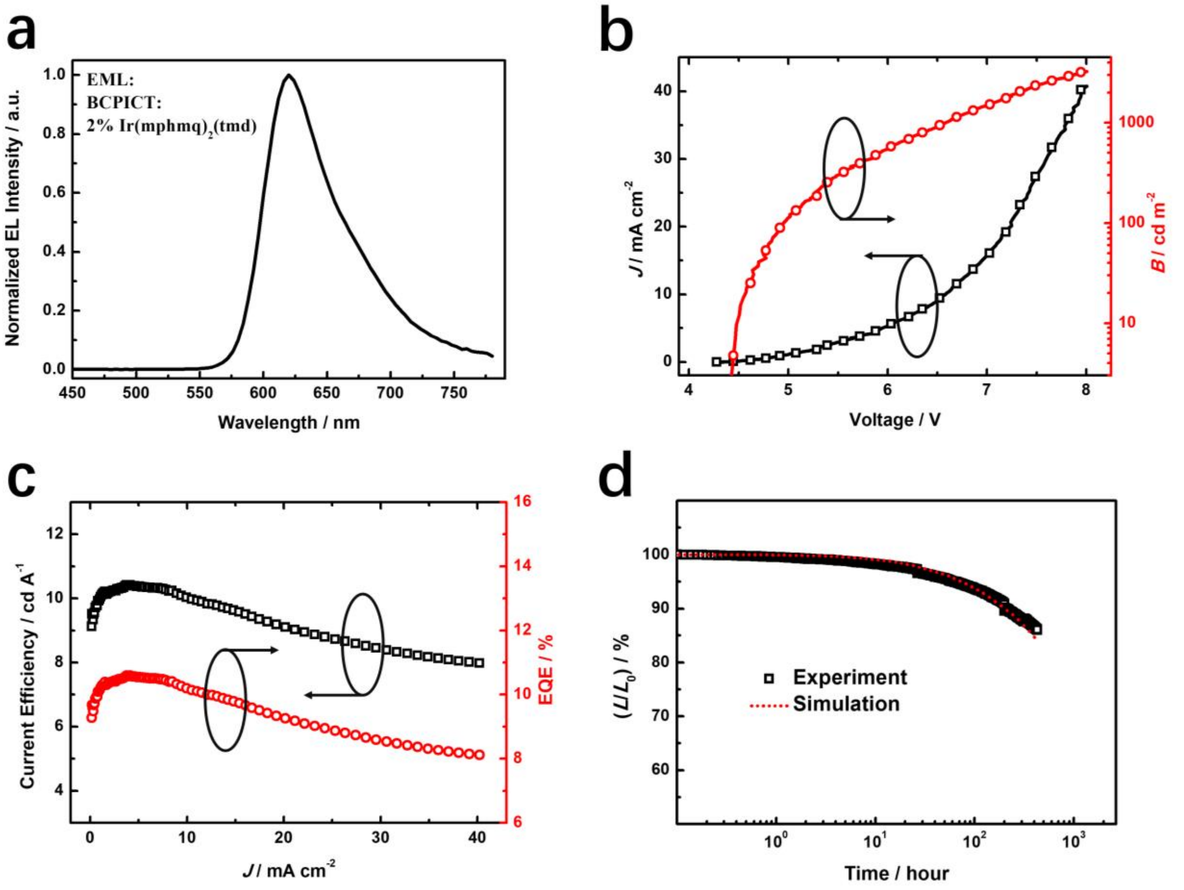

Figure S12. Performance of OLED device with structure of ITO substrate (80 nm) / HAT-CN (5 nm) / NPB (30 nm) / TCTA (10 nm) / BCPICT : 2 wt % Ir(mphmq)$_2$(tmd) (30 nm) / TPBi (30 nm) / LiF (1 nm) / Al (150 nm). (a) EL spectra, (b) J-V-L curves, (c) current efficiency - J and EQE-J curves, and (d) experimental and simulated luminance loss curve, at an initial luminance of 4000 cd m^{-2}. ΔE_{ST} of 0.055 eV and k_{ET} from **Table S2** were used in the simulation.

10. Absorption and PL Emission Spectra of Various Neat Films.

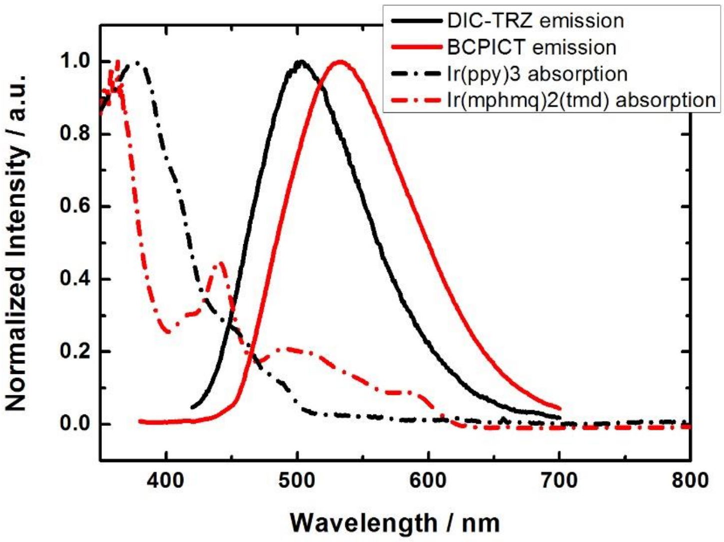

Figure S13. The PL emission spectra of host materials DIC-TRZ and BCPICT, along with the absorption spectra of Ir(ppy)$_3$ and Ir(mphmq)$_2$(tmd) phosphors, all tested in films.

References

1 Y. S. Shin, K. Lee, Y. R. Kim, H. Lee, I. M. Lee, W. T. Kang, B. H. Lee, K. Kim, J. Heo, S. Park, Y. H. Lee and W. J. Yu, *Adv. Mater.*, 2018, **30**, 1704435.

2 F.-C. Chiu, *Adv. Mater. Sci. Eng.* 2014, **2014**, 18.

3 N. C. Giebink, B. W. D'Andrade, M. S. Weaver, J. J. Brown and S. R. Forrest, *J. Appl. Phys.*, 2009, **105**, 124514.

4 D. Zhang, L. Duan, C. Li, Y. Li, H. Li, D. Zhang and Y. Qiu, *Adv. Mater.*, 2014, **26**, 5050-5055.

5 C. Adachi, *Jpn. J. Appl. Phys.*, 2014, **53**, 060101.

6 C. Li, L. Duan, D. Zhang and Y. Qiu, *ACS Appl. Mater. Interfaces*, 2015, **7**, 15154-15159.

7 A. S. D. Sandanayaka, T. Matsushima and C. Adachi, *J. Phys. Chem. C*, 2015, **119**, 23845-23851.